Journal of Power Sources 205 (2012) 500–505

Contents lists available at SciVerse ScienceDirect

Journal of Power Sources

journal homepage: www.elsevier.com/locate/jpowsour

In situ investigation of the volume change and pulverization of hydride materials for Ni-MH batteries by concomitant generated force and acoustic emission measurements

A. Etiemble[a,b], H. Idrissi[a,*], S. Meille[a], L. Roué[b,**]

[a] INSA-Lyon, MATEIS CNRS UMR5510, F-69621 Villeurbanne, France
[b] INRS-Énergie, Matériaux et Télécommunications, Varennes, Québec J3X 1S2, Canada

ARTICLE INFO

Article history:
Received 8 November 2011
Received in revised form 5 January 2012
Accepted 6 January 2012
Available online 16 January 2012

Keywords:
Ni-MH batteries
Metal hydride electrodes
Volume expansion
Particle cracking
Compression load cell
Acoustic emission

ABSTRACT

A new experimental set-up constituted of an electrochemical cell connected to a compression load cell and acoustic emission (AE) equipment was used for monitoring the force and the cracking of metal hydride electrodes generated by their volume expansion/contraction during their cycling. Two materials were studied: a commercial $LaNi_5$-based alloy and an amorphous MgNi alloy prepared by ball milling. During the charge of the $LaNi_5$-based electrode, a concordance was observed between the increase of the force generated by its volume expansion and the increase of the AE activity associated with the particle cracking. This correlation was not observed during the charge of the MgNi electrode, which tends to confirm that the main origin of the cracking of the MgNi particles is not their volume expansion but is rather due to the mechanical action of the H_2 bubbles produced at the end of the charge step. In addition, on the basis of the generated/relaxed force rates, the volume expansion/contraction of the electrode appeared more progressive with the MgNi alloy than with the $LaNi_5$-based alloy. This could result from the lack of abrupt α–β phase transition region in the MgNi alloy due to its amorphous structure.

1. Introduction

In recent years, magnesium-based alloys have been extensively studied as active materials in negative electrodes for nickel-metal hydride (Ni-MH) batteries because they present a high theoretical hydrogen absorption capacity in addition to be inexpensive and environmentally friendly. For example, amorphous MgNi alloy obtained by high-energy ball-milling has an initial discharge capacity close to 500 mAh g^{-1} [1], compared to ~300 mAh g^{-1} for $LaNi_5$-based alloys used in commercial Ni-MH batteries. The poor cycle life of the MgNi electrode, however, prevents its commercial use. This is mainly due to the irreversible oxidation of the MgNi alloy by the KOH electrolyte [2]. This process is strongly accelerated by the pulverization of the MgNi particles occurring during the hydrogen absorption/desorption cycles [3]. For $LaNi_5$-based alloys, the pulverization phenomenon induces the electrode activation by breaking the native surface oxide layer and by increasing the effective surface area of the electrode [4]. But it also decreases their cycle life by increasing the alloy corrosion rate [5]. The pulverization of the $LaNi_5$-based electrodes results from the large discrete lattice expansion (typically, 10–20 vol.%) between the α-solid solution and β-hydride phase as shown from *in situ* X-ray diffraction analyses [6–8].

Acoustic emission (AE) is a nondestructive technique, which enables *in situ* study of the hydrogen evolution reaction (HER) and mechanical damage during corrosion of various materials [9–11]. We have recently demonstrated by coupling electrochemical measurements with AE that MgNi and $LaNi_5$-based alloys present different pulverization mechanisms [12]. The pulverization of the MgNi electrode mainly occurs at the end of the charge step (i.e., when the HER is initiated) whereas for the $LaNi_5$-based electrode, its cracking is observed at the beginning of the charge (i.e., in the α-to-β phase transition zone). This difference between the pulverization mechanisms is explained by the porous morphology and amorphous structure of the MgNi powder compared to the dense and crystalline $LaNi_5$-based material. Indeed, the MgNi material consists of porous agglomerates made up of many particles cold-welded together, which are likely to be easily broken down by the mechanical action of the H_2 bubbles during the HER. On the other hand, its volume expansion during hydrogen absorption is assumed to be lower and more progressive than for the crystalline $LaNi_5$-based alloy due to its amorphous structure. However, this latter

* Corresponding author at: INSA-Lyon MATEIS CNRS UMR5510, F-69621 Villeurbanne, France. Tel.: +33 4 72 43 89 20; fax: +33 4 72 73 87 15.
** Corresponding author at: INRS-Énergie, Matériaux et Télécommunications, 1650, bd. Lionel Boulet, Varennes, Québec J3X 1S2, Canada. Tel.: +1 450 929 8185; fax: +1 450 929 8102.
E-mail addresses: hassane.idrissi@insa-lyon.fr (H. Idrissi), roue@emt.inrs.ca (L. Roué).

0378-7753/$ – see front matter © 2012 Elsevier B.V. All rights reserved.
doi:10.1016/j.jpowsour.2012.01.066

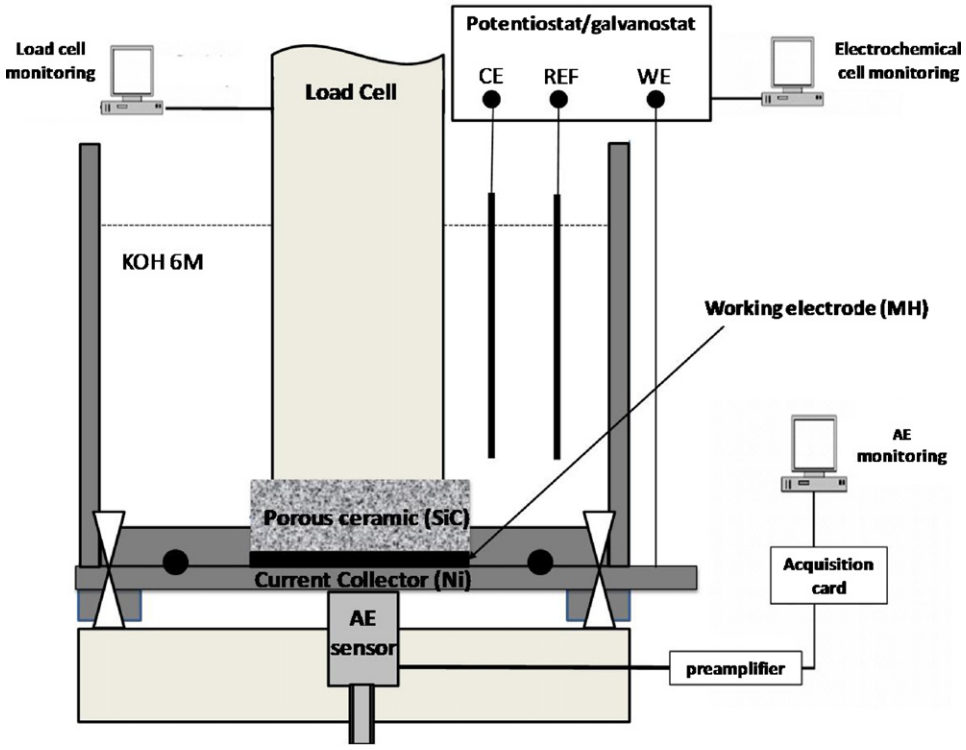

Fig. 1. Schematic diagram of the experimental set-up for concomitant electrochemical, generated stress, and acoustic emission measurements.

assumption cannot be confirmed from *in situ* XRD investigations due to the amorphous structure of MgNi.

In the present study, we propose to correlate the detected AE activity with the force generated/relaxed by the volume expansion/contraction of $LaNi_5$-based and MgNi electrodes during cycling. The primary objective is to determine if the generated force and thus indirectly the volume expansion related to H-absorption is lower and more progressive on MgNi than on the $LaNi_5$-based alloy. For that purpose, a new experimental set-up constituted of a compression load cell (similar to that used in studies of the exfoliation corrosion of Al-based alloys [10,13]) connected to electrochemical and AE equipment was conceived. To our knowledge, this is the first time that this set-up has been applied to the study of Ni-MH battery materials.

2. Experimental

A commercial $LaNi_5$-based alloy ($MmNi_{3.68}Co_{0.78}Mn_{0.36}Al_{0.28}$) powder from Japan Metals & Chemicals Co and an amorphous MgNi alloy powder obtained by high energy ball milling [1] were studied as active materials. 0.2 g of active material was manually mixed with 0.2 g of copper powder. The mixture was then cold pressed on 2 g of copper powder at 6 tons cm^{-2} for 10 min in a stainless steel die to form a pellet (16 mm in diameter, ~2 mm in thickness) used as working electrode.

The experimental set-up used for concomitant electrochemical, AE, and stress measurements is schematized in Fig. 1. The reference and counter electrodes were an Hg/HgO electrode and a nickel wire, respectively. The three-electrode cell was monitored by a Voltalab PGZ 301 galvanostat/potentiostat. Unless otherwise indicated, the working electrode was charged at $-100\ mA\ g^{-1}$ for 3 h (charge input of $300\ mAh\ g^{-1}$) for the $LaNi_5$-based alloy and 5 h (charge input of $500\ mAh\ g^{-1}$) for MgNi, and discharged at $20\ mA\ g^{-1}$ until reaching −0.6 V vs. Hg/HgO. All the experiments were carried out at room temperature in a $6\ mol\ L^{-1}$ KOH solution. Before the first charge, the potential of the working electrode was maintained at −0.85 V vs. Hg/HgO for a few minutes to reduce the native oxide layer present on the Cu and active material powders.

The AE signals were recorded during cycling by a wide band sensor EPA micro 80 (frequency range 100–1000 kHz) and transmitted via an EPA USB Node acquisition card to the computer. For all the experiments, the gain *G* and the threshold *S* were fixed at 40 dB and 27 dB, respectively. The recorded acoustic signals were treated and the waveforms were obtained with AE Win software (EPA). The AE signals are separated into two classes. The first one, labeled P1, is attributed to cracking of MH particles and the second one, labeled P2, is due to the release of H_2 bubbles [12,14]. The temporal and energetic characteristics of both signal types were described in detail in Ref. [12]. In the present study, the P1 and P2 activities (number of events) were normalized to their maximum value measured at the end of the charge step.

The force generated during charge/discharge cycling was measured by a 500 N compression load cell, mounted on an Instron 1195 equipment. An increase (decrease) in force indicated a volume expansion (contraction) of the working electrode. In order to ensure the contact between the working electrode and the electrolyte, a SiC ceramic pellet (16 mm in diameter, 8 mm in thickness) with a porosity of 60% was placed between the working electrode and the load cell. A small compressive pre-load of 2 N was applied on the working electrode beforehand in all tests. The same experiments were repeated at least three times to check their reproducibility.

3. Results and discussion

3.1. Evolution of the AE activity and generated force during the first charge

The evolution of the electrode potential, generated force, and normalized acoustic activities of P1 and P2 type AE signals as a function of the charge input during the first charge are shown in Fig. 2A and B for the $LaNi_5$-based and MgNi electrodes, respectively.

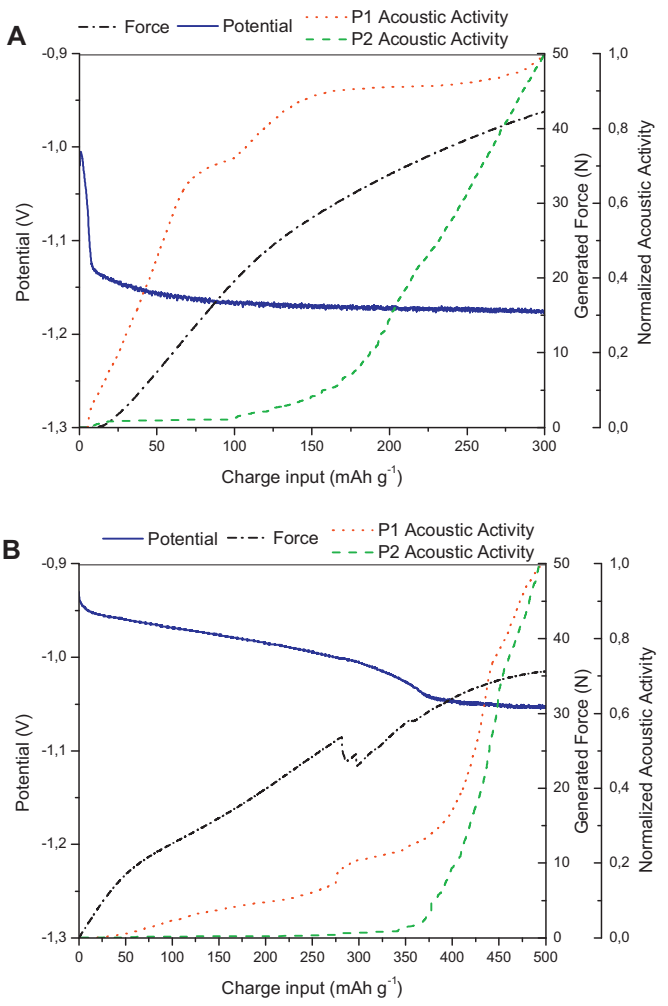

Fig. 2. Evolution of the electrode potential, the normalized P1 and P2-type acoustic activities and the generated force as a function of the charge input on (A) $LaNi_5$-based electrode and (B) MgNi electrode during the first charge.

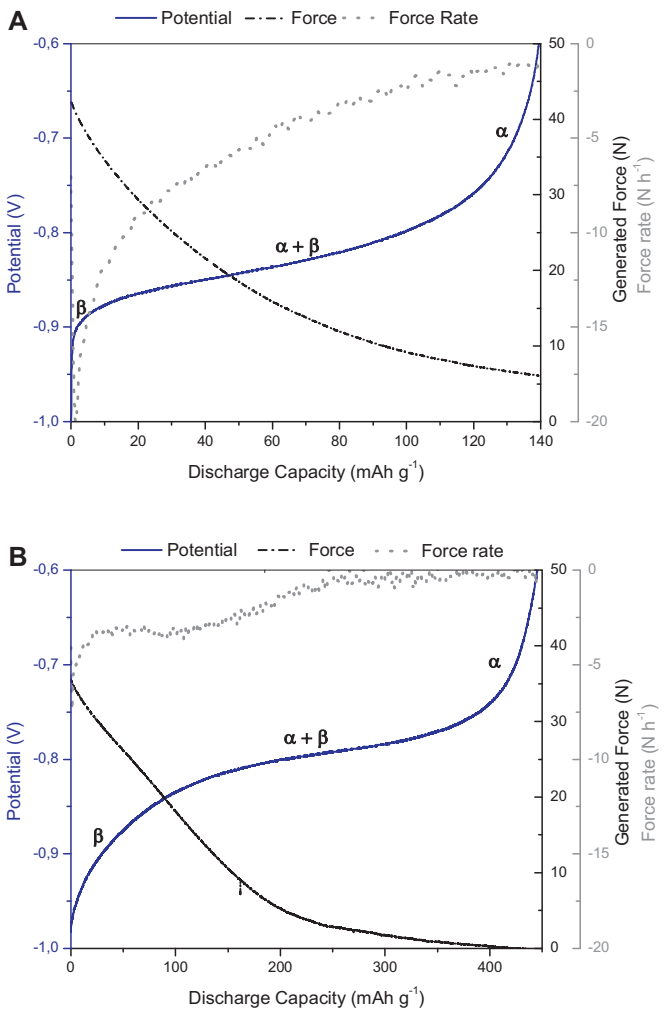

Fig. 3. Evolution of the electrode potential, the relaxation force, and the force relaxation rate as a function of the discharge capacity on (A) $LaNi_5$-based electrode and (B) MgNi electrode during the first discharge.

In the case of the $LaNi_5$-based electrode (Fig. 2A), a rapid decrease of the electrode potential, probably related to the native oxide layer reduction, is observed up to a charge input of 5 mAh g^{-1}. No force is generated and no acoustic activity is detected during this short period. As the charge input increases, a slow decrease of the electrode potential associated with the hydrogen absorption reaction (HAR) is observed and tends to stabilize around −1.17 V vs. Hg/HgO. From a charge input of ~100 mAh g^{-1}, the hydrogen evolution reaction (HER) occurs concomitantly with the HAR and becomes dominant from a charge input of ~170 mAh g^{-1}. This is consistent with the evolution of the P2-type AE activity (related to the release of H_2 bubbles [12]), which slightly increases from a charge input of ~100 mAh g^{-1} and abruptly rises from a charge input of ~170 mAh g^{-1}. Regarding the evolution of the P1-type AE activity (related to the MH particle cracking [12]), a large increase is observed from 5 to ~60 mAh g^{-1} followed by a second and less important increase from ~100 to ~150 mAh g^{-1}. Almost no P1-type AE activity is detected at a charge input >150 mAh g^{-1}. As shown previously [12], the first large increase of the P1 activity is due to the MH particle cracking resulting from the α-to-β phase transition, which induces an abrupt lattice expansion [6–8]. The second increase initiated at ~100 mAh g^{-1} (corresponding to the beginning of the HER) was not observed in our previous AE study [12] and could result from the accumulation of H_2 bubbles in the electrode pores and between the working electrode and the ceramic pellet of the compression load cell (see Fig. 1), which may favor the cracking of the electrode. Regarding the evolution of the generated force, it rises rapidly when the charge input increases from ~10 to ~100 mAh g^{-1} and then slows to reach a maximum value of 42 N (corresponding to a stress of 0.21 MPa over the electrode with a contact surface area of 2 cm^2) at the end of the charge step. The measured force could be generated by (i) the alloy volume expansion associated with the formation of the β-hydride phase, (ii) the formation of voluminous corrosion products such as $Mm(OH)_3$ [15], or (iii) the pressure exerted on the load cell by the accumulation of H_2 bubbles as discussed before. A small decrease of the generated force (~7 N) due to the evacuation of the H_2 bubbles was observed after the charge step in open-circuit conditions for 5 h (not shown). This tends to confirm that the generated force is mainly due to the formation of the β-hydride phase. This is in accordance with the fact that the force is mainly generated at the beginning of the charge, i.e. when an abrupt lattice expansion due the α-to-β phase transition occurs [6–8]. Moreover, a concordance appears between the increase of generated force and the increase of the P1 activity, confirming that the cracking of the $LaNi_5$-based particles is due to their volume expansion. Note that the generated force does not reach a plateau value at the end of the charge step, probably because the hydriding of the $LaNi_5$-based electrode is not fully completed after the first charge.

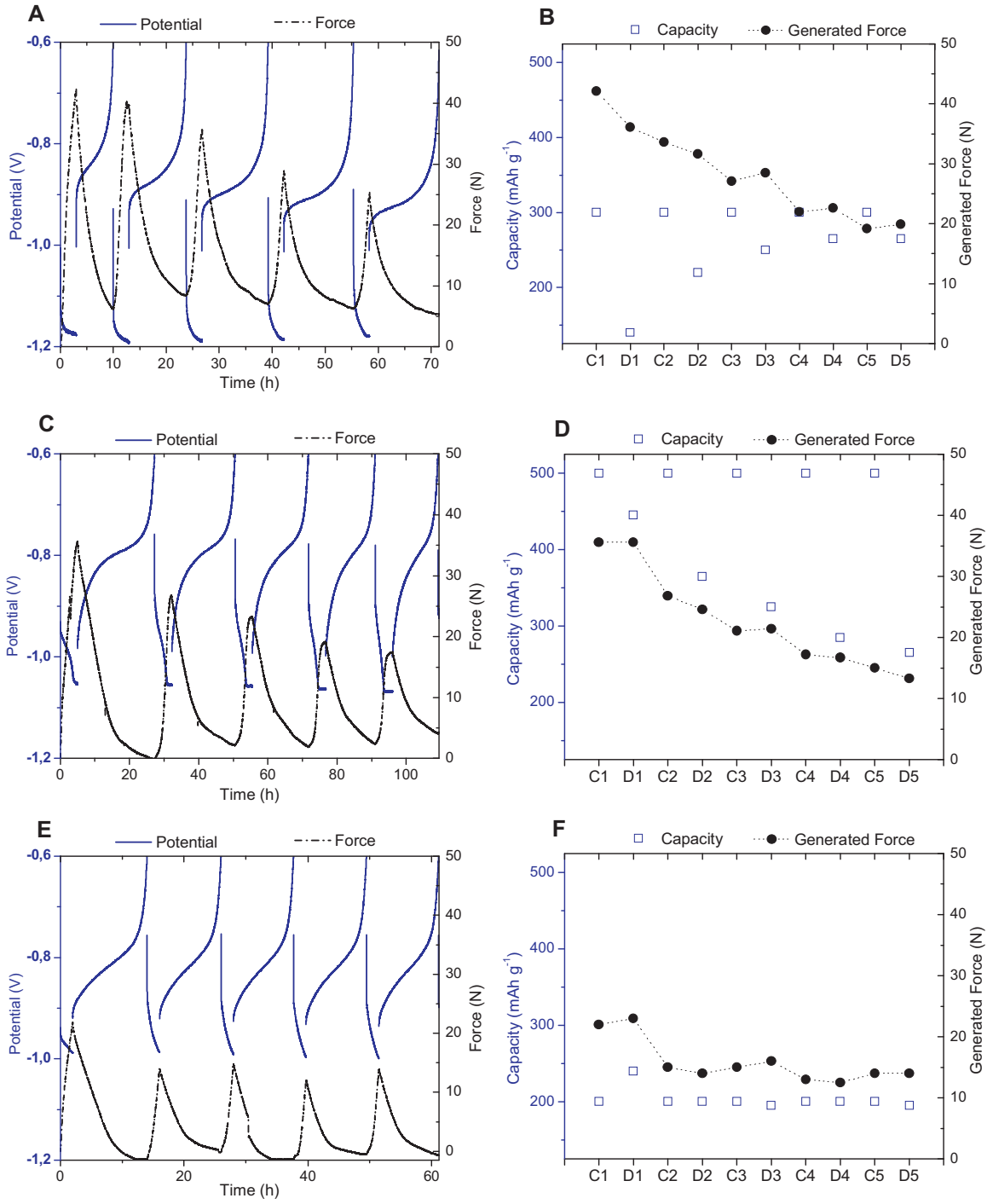

Fig. 4. Evolution of the charge/discharge potential curves and the expansion/relaxation force curves during the first five cycles on (A) $LaNi_5$-based electrode charged to 300 mAh g^{-1}, (C) MgNi electrode charged to 500 mAh g^{-1}, and (E) MgNi electrode charged to 200 mAh g^{-1}. The electrode capacities and generated forces extracted from these curves are shown in Fig. 4B, D, and F, respectively.

On the MgNi electrode (Fig. 2B), a slow decrease of the electrode potential from −0.93 to −1.05 V vs. Hg/HgO related the HAR is observed as the charge input increases up to ~375 mAh g^{-1}. At higher charge inputs, the electrode potential stabilizes around −1.05 V vs. Hg/HgO due to the HER as confirmed by the abrupt increase of the P2 acoustic activity from ~375 mAh g^{-1}. In contrast to what was previously observed on the $LaNi_5$-based electrode, the P1 acoustic activity is low in the HAR region and becomes important only when the HER is dominant, i.e. from ~375 mAh g^{-1}. As explained in Section 1 and in our recent AE study [12], this indicates that the cracking of the MgNi particles mainly results from the mechanical action of the H_2 bubbles produced at the end of the charge step through the HER rather than to the alloy volume expansion related to the HAR. On the other hand, the generated force (stress) quickly increases up to 10 N (0.05 MPa) in the first 50 mAh g^{-1}. This is attributed to the volume expansion associated with the α-to-β phase transition rather than the $Mg(OH)_2$ formation, because an identical generated force has been measured during the first charge even when the electrode was previously left in open-circuit for 24 h in KOH solution (not shown). From a charge

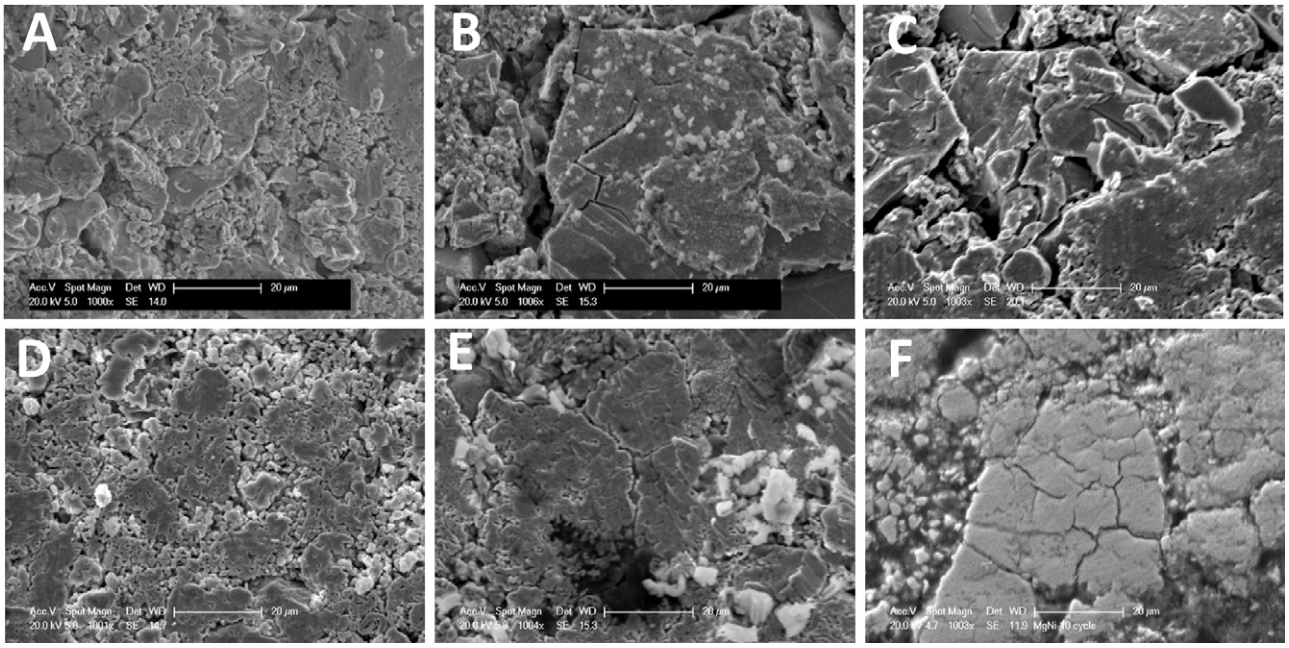

Fig. 5. SEM micrographs of a $LaNi_5$-based electrode before charging (A), after 1 cycle (B), after 4 cycles (C) and of a MgNi electrode before charging (D), after 1 cycle (E), and after 10 cycles (F).

input of 50 mAh g^{-1}, the generated force progressively increases to reach a plateau value of 36 N (0.18 MPa) at the end of the charge. Note that a short stress relaxation and an increase of the P1 activity are observed at ~275 mAh g^{-1}, which could be related to the formation of a macroscopic crack in the electrode. In comparison with the $LaNi_5$-based electrode (Fig. 2A), there is no apparent correlation between the increase of the generated force and the increase of the P1 activity during charging, which tends to confirm that the main origin of the cracking of the MgNi particles is not their volume expansion, as previously stated. Moreover, the increase of the generated force associated with H-absorption is more progressive and slightly lower on the MgNi electrode (Fig. 2B) than on the $LaNi_5$-based electrode (Fig. 2A) despite the larger amount of hydrogen absorbed in the former. This could be explained by the lack of an abrupt α-β phase transition region in the MgNi alloy due to its amorphous structure, as argued in Section 1.

3.2. Evolution of the generated force during the first discharge

The evolution of the electrode potential, the generated force, and the rate of the generated force during the first discharge on the $LaNi_5$-based and MgNi electrodes are shown in Fig. 3A and B, respectively. No significant acoustic activity was detected during the discharge.

In the case of the $LaNi_5$-based electrode (Fig. 3A), the electrode potential increases from −0.91 to −0.60 V vs. Hg/HgO with a large and well-discernable plateau centered around −0.83 V corresponding to the α+β mixed region. The generated force (stress) decreases from 42 N (0.21 MPa) to 6 N (0.03 MPa) due to the alloy volume contraction associated with the hydrogen desorption reaction. The generated force does not reach zero at the end of discharge, which may indicate that H-desorption from the $LaNi_5$-based alloy is incomplete. The evolution of the generated force rate clearly shows that the volume contraction is rapid during the first 20 mAh g^{-1} with a rate of 10–20 N h^{-1} and progressively slows as the depth of discharge increases. These observations corroborate those obtained by *in situ* neutron diffraction studies of $LaNi_5$-based alloys [16,17], which show a rapid volume contraction at the beginning of the discharge (β phase region) followed by a slow volume contraction when the desorption plateau (α+β phase region) is reached. Such behavior is explained by kinetic limitations related to the mobility of the α/β interface [17].

In the case of the MgNi electrode (Fig. 3B), an increase of the electrode potential from −0.97 to −0.60 V vs. Hg/HgO related to the hydrogen desorption reaction is observed. As previously seen on the $LaNi_5$-based electrode, a desorption plateau centered around −0.80 V is also well discernible. However, compared with the $LaNi_5$-based alloy, an extension of the single β-phase and α-phase regions leading to the narrowing of the α+β phase region is clearly apparent, which agrees with the amorphous structure of the MgNi alloy. The generated force decreases almost linearly from 36 to 8 N at a mean rate of ~3 N h^{-1} up to a discharge capacity of ~170 mAh g^{-1}, which corresponds to the beginning of the α+β phase region. Then, the rate of the generated relaxation force greatly slows down and the force reaches 0 N at the end of the discharge. As previously argued for the $LaNi_5$-based, the abrupt decrease of the rate of the relaxed force when the MgNi electrode reaches the α+β phase region could reflect an H-desorption process kinetically limited by the α↔β phase transformation (i.e., by the mobility of the α/β interface). Lastly, on the basis of their respective force relaxation rates, the volume contraction appears much slower with MgNi than with the $LaNi_5$-based alloy, even in the β phase region.

3.3. Evolution of the generated force with cycling

Fig. 4 shows the evolution of the charge/discharge potential curves and the generated/relaxed force curves during the first five cycles for the $LaNi_5$-based electrode charged to 300 mAh g^{-1} (Fig. 4A) and MgNi electrodes charged to 500 (Fig. 4C) and 200 mAh g^{-1} (Fig. 4E). The electrode capacities and generated forces extracted from these curves are shown in Fig. 4B, D and F, respectively.

For the $LaNi_5$-based electrode (Fig. 4A and B), the discharge potential decreases and the discharge capacity increases (from 140 to 265 mAh g^{-1}) with cycling, reflecting the well-known activation of the electrode related to the particle cracking [6] as explained in

Section 1. On the other hand, a progressive decrease of the maximum generated force (from 42 to 20 N) is observed with cycling. This is in contradiction with the concomitant increase of the electrode H-storage capacity, which should induce an increase of the generated force due to a higher volume expansion/contraction of the $LaNi_5$-based alloy. Actually, the observed decrease of the generated force with cycling may be due to the increase of the electrode porosity resulting from the particle cracking, as shown in the SEM images of cycled $LaNi_5$-based electrodes (Fig. 5B and C). This porosity may act as a buffer volume during the alloy expansion. The volume expansion of the particles is therefore not detected macroscopically by the generated force measurement until the pores are filled. In this way, the maximum generated force decreases and appears at a higher charge input with cycling, as shown in Fig. 4A. It can also be noted in Fig. 4A that the difference between the generated expansion force (charge step) and the relaxation force (discharge step) decreases from 6 to 0 N with cycling, reflecting the improvement of the electrode reversibility through its activation.

In the case of the MgNi electrode (Fig. 4C and D), its discharge capacity decreases rapidly with cycling (from 445 to 265 mAh g^{-1} in the first 5 cycles) due to its irreversible oxidation by the KOH electrolyte leading to the formation of $Mg(OH)_2$ [2]. The maximum generated force also decreases with cycling (from 36 to 13 N) in accordance with the decrease of the electrode H-storage capacity. This decay can also result from the increasing electrode porosity generated with the particle cracking (see Fig. 5E and F), as explained previously for the $LaNi_5$-based electrode. In addition, a progressive increase of the remaining force measured at the end of the discharge is discernable with cycling (from 0 to 4 N as seen in Fig. 4C). This can be explained by the growth of the $Mg(OH)_2$ layer on the particles with cycling. In contrast, when the charge input of the MgNi electrode is limited to 200 mAh g^{-1} (Fig. 4E and F) in order to prevent major particle cracking (see P1 acoustic activity in Fig. 2B), no significant capacity decay with cycling is observed. Moreover, the maximum generated force remains almost stable (∼15 N) from the second cycle and the generated force is fully relaxed cycle after cycle, indicating that no particle cracking and no $Mg(OH)_2$ growth occurred under such conditions. These observations tend to confirm the correlation existing between the MgNi particle cracking favoring the $Mg(OH)_2$ formation and the degradation of the electrode capacity.

4. Conclusion

This study demonstrated that the coupling of electrochemical, acoustic emission, and stress measurements is an effective method for the *in situ* characterization of the volume change and the pulverization of hydride materials for Ni-MH batteries. Thanks to this method, it has been demonstrated that the generated/relaxed stress associated with the electrode volume expansion/contraction during hydrogen absorption/desorption cycling is more progressive on the amorphous MgNi electrode than on the crystalline $LaNi_5$-based electrode. Further AE experiments on Ni-MH batteries during normal and abusive (e.g., overcharge) conditions are planned with the aim of developing a new diagnostic and battery management tool based on AE measurements.

Acknowledgments

The authors thank the Natural Science and Engineering Research Council (NSERC) of Canada and the *Commission permanente de coopération franco-québécoise* for supporting this work.

References

[1] S. Ruggeri, C. Lenain, L. Roué, G. Liang, J. Huot, R. Schulz, J. Alloys Compd. 339 (2002) 195–201.
[2] S. Ruggeri, L. Roué, J. Huot, R. Schulz, L. Aymard, J.M. Tarascon, J. Power Sources 112 (2002) 547–556.
[3] S. Ruggeri, L. Roué, J. Power Sources 117 (2003) 260–266.
[4] P.H.L. Notten, R.E.F. Einerhand, J.L.C. Daams, J. Alloys Compd. 210 (1994) 221–232.
[5] J.J.G. Willems, Philips J. Res. 39 (1984) 1–94.
[6] P.H.L. Notten, J.L.C. Daams, R.E.F. Einerhand, J. Alloys Compd. 210 (1994) 233–241.
[7] P.H.L. Notten, R.E.F. Einerhand, J.L.C. Daams, J. Alloys Compd. 231 (1995) 604–610.
[8] Y. Nakamura, K. Sato, S. Fujitani, K. Nishio, K. Oguro, I. Uehara, J. Alloys. Compd. 267 (1998) 205–210.
[9] H. Idrissi, J. Derenne, H. Mazille, Proceedings of the 24th European Conference on Acoustic Emission Testing EWGAE, Paris, France, 2000, pp. 409–416.
[10] F. Bellenger, H. Mazille, H. Idrissi, NDT & E Int. 35 (2002) 385–392.
[11] M. Perrin, L. Gaillet, C. Tessier, H. Idrissi, Corros. Sci. 52 (2010) 1915–1926.
[12] A. Etiemble, H. Idrissi, L. Roué, J. Power Sources 196 (2011) 5168–5173.
[13] D. McNaughtan, M. Worsfold, M.J. Robinson, Corros. Sci. 45 (2003) 2377–2389.
[14] S. Didier-Laurent, H. Idrissi, L. Roué, J. Power Sources 179 (2008) 412–416.
[15] F. Maurel, B. Knosp, M. Backhaus-Ricoult, J. Electrochem. Soc. 147 (2000) 78–86.
[16] M. Latroche, A. Percheron-Guegan, Y. Chabre, J. Bouet, J. Pannetier, E. Ressouche, J. Alloys Compd. 231 (1995) 537–545.
[17] M. Latroche, Y. Chabre, B. Decamps, A. Percheron-Guegan, J. Alloys Compd. 334 (2002) 267–276.